International Journal of Heat and Fluid Flow 29 (2008) 1125–1138

Contents lists available at ScienceDirect

International Journal of Heat and Fluid Flow

journal homepage: www.elsevier.com/locate/ijhff

Numerical and experimental investigation of laminar free convection around a thin wire: Long time scalings and assessment of numerical approach

Marie-Christine Duluc [a], Shihe Xin [b], François Lusseyran [a], Patrick Le Quéré [a,*]

[a] LIMSI-UPR CNRS, BP 133, 91403 Orsay Cedex, France
[b] Cethil, UMR 5008, INSA-Lyon, 9, Rue de la Physique, 69621 Villeurbanne, France

ARTICLE INFO

Article history:
Received 18 September 2007
Received in revised form 4 February 2008
Accepted 8 February 2008
Available online 7 April 2008

Keywords:
External free convection
Heat source
Scaling laws
Numerical and experimental study
Artificial boundary conditions

ABSTRACT

Transient and steady free convection around a line heat source is studied experimentally and numerically. Experiments are performed with a thin platinum wire of 50 μm in radius immersed in water and heated by Joule effect. Time evolution of velocity and temperature fields are measured by PIV (Particle Image Velocimetry) and micro-thermocouple for three different heating rates. Numerical simulations are done using a time-stepping algorithm based on a velocity–pressure formulation. The equations are discretized on a domain of limited extension, using spectral type approximations and a domain decomposition technique, and a pressure condition is imposed at the outer boundary. A three-stage scenario is proposed for the development of transient free convection around a thin wire, and, at each stage, the numerical approach is assessed through detailed comparison between numerical and experimental results. Previously established scaling laws for the onset of convective motion are checked for long time behavior. Numerical and experimental results confirm that these laws remain meaningful at long time and a qualitative similarity is observed for the transients. In addition, a steady case of a heated wire in air is studied and compared with the experimental study of Brodowicz and Kierkus [Brodowicz, K., Kierkus, W., 1966. Experimental investigation of free-convection in air above horizontal wire with constant flux. Int. J. Heat Mass Trans. 9, 81–94]. Despite a wire superheat of 210 K, good agreement is observed between the experiment and numerical simulations performed under the Boussinesq assumption. In particular, numerical simulations match with the scaling laws of the far-field above the wire.

1. Introduction

Owing to its importance in many engineering or natural configurations, external natural convection or free convection around a heat source has long been the subject of active research (see Turner (1979); Gebhart (1988)). Most investigations have been carried out using either analytical or experimental approaches. Somewhat surprisingly, despite their overwhelming importance in today's research on heat & mass transfer and fluid mechanics, numerical investigations remain relatively rare. This strongly differs from internal natural convection (in rectangular cavities, for example) for which the number of numerical studies is very large. This disparity likely comes from the fact that for internal natural convection the geometry as well as the boundary conditions are known. In contrast, when dealing with free convection, one has to face these two issues, *i.e.*, the choice of the size of the computational domain and the nature of the boundary conditions. As the flow of interest takes place in an unbounded or very large domain, the boundary of the computational domain can no longer correspond to a physical limit. A natural choice may seem to use a bounded but still very large computational domain. This was chosen by Saitoh and co-workers (Saitoh et al., 1993) to study the benchmark problem of steady free convection around an isothermal cylinder. The computational domain is 1000–20,000 times the cylinder diameter and solid type boundary conditions (ambient temperature and no-slip for velocity) are imposed at the outer boundary. The main drawback of this approach is the prohibitive computation cost. An alternative is to use a computational domain of smaller reasonable extension. This is a challenging situation because one has to derive artificial boundary conditions on the outer edge of the computational domain, where inflow and outflow conditions occur at the same time, with the additional complexity that the inflow and outflow parts may vary in time. Furthermore, these artificial boundary conditions should address both dynamical and thermal aspects, in particular for unsteady simulations.

Previous numerical works available in the literature have principally focused on steady flows (Saitoh et al., 1993; Kuehn and Goldstein, 1980; Farouk and Güçeri, 1981; Wang et al., 1990; Kelkar and Choudhury, 2000; Linan and Kurdyomov, 1998; Corcione, 2005). A benchmark problem (Saitoh et al., 1993) was proposed for steady flows around an isothermal cylinder because flow

* Corresponding author. Tel.: +33 169858085.
E-mail address: plq@limsi.fr (P. Le Quéré).

0142-727X/$ - see front matter © 2008 Elsevier Inc. All rights reserved.
doi:10.1016/j.ijheatfluidflow.2008.02.012

Nomenclature

C_p	specific heat of working liquid at constant pressure (J kg^{-1} K^{-1})
$\widetilde{C}$	specific heat of the wire (J kg^{-1}K^{-1})
g	gravity acceleration (m/s^2)
h	heat transfer coefficient (W m^{-2} K^{-1})
Pr	Prandtl number ($= \nu/\kappa$)
p	pressure deviation from hydrostatic pressure (Pa)
q	heat flux (W m^{-2})
Q	heat power (W)
r	radial distance (m)
R	wire radius (m)
R'	radial position of the outer boundary (m)
Ra	Rayleigh number ($= (g\beta qR^4)/(\nu\kappa\lambda)$)
t	time (s)
T	temperature (K)
u	radial velocity component (m/s)
u	horizontal velocity component (m/s)
v	azimuthal velocity component (m/s)
v	vertical velocity component (m/s)
x	horizontal position (m)
y	vertical position (m)
β	coefficient of volumetric thermal expansion (K^{-1})
$\Delta T = T - T_0$	superheat (K)
κ	thermal diffusivity (m^2/s)
λ	thermal conductivity of working liquid (W m^{-1} K^{-1})
$\widetilde{\lambda}$	thermal conductivity of the wire (W m^{-1} K^{-1})
μ	dynamic viscosity of working liquid (kg m^{-1} s^{-1})
ν	kinematic viscosity of working liquid (m^2/s)
ρ	density of working liquid (kg/m^3)
$\widetilde{\rho}$	wire density (kg/m^3)
θ	azimuthal position in polar system

Subscripts

v	volumetric (per volume)
0	related to initial or ambient condition
1, 2, 3	related to heating rates or transient stages

surrounding the heating element becomes rapidly steady. This benchmark is based uniquely on heat transfer as results concentrate on local and mean Nusselt numbers and no information was provided on velocity field. In our previous studies (Duluc et al., 2003; Xin et al., 2004), we performed numerical simulations for this benchmark problem by considering a limited computational domain and testing two different sets of outer boundary conditions. A very good agreement with reference results of the benchmark problem was achieved in both cases in terms of heat transfer. However, the flow structures displayed significant differences resulting from the different boundary conditions used. This indicates that the assessment of numerical methodologies to perform simulations of external free convection cannot be entirely realized by a single criterion based on heat transfer. This comparison requires in particular detailed experimental information on flow structure of free convection.

To our knowledge, there are very few studies in the open literature which have addressed detailed investigation of transient flow structure. The pioneering experimental work of Ostroumov (1956) used a platinum wire and was concerned with visualization of both velocity and temperature fields but no quantitative results were provided. As no experimental results of velocity and temperature fields were found in the literature and due to the pressing need for experimental measurements to qualify numerical simulations of transient free convection and to provide physical quantities necessary for assessing numerical approaches, an experiment around a line heat source was set up (Xin et al., 2004). PIV (Particle Image Velocimetry) techniques were used to give quantitative access of transient flow structures. In this study Xin et al. (2004), the numerical methods used and their implementation have been detailed, numerical simulations have been performed and comparison of numerical results with experimental measurements allowed validating the outer boundary conditions employed. However, it was shown that numerical results cannot be satisfactory everywhere in the computational domain during the whole transient due to the artificial feature of the outer boundary conditions.

Recently, the pioneering experimental study of Brodowicz and Kierkus (1966) came to our attention. This study, focused on air flow around a thin wire heated by Joule effect, was entirely devoted to steady flow and provided experimental data of both the flow and temperature fields. The temperature field was measured by a Mach-Zehnder interferometer. Streamlines were determined from dust particles and the velocity along the streamlines were computed from snapshots using stroboscopes. Since our previous studies (Duluc et al., 2003; Xin et al., 2004) were conducted without knowledge of the work by Brodowicz and Kierkus (1966), the present work is at least motivated by performing numerical simulations for the same configuration as in Brodowicz and Kierkus (1966), and checking the validity of our numerical approach from detailed comparisons. Let us again emphasize that Brodowicz and Kierkus (1966) measured both temperature and velocity fields, the latter being of utmost importance for validating applications of numerical methods to free convection.

The aim of the present paper is to extend our previous work on transient free convection induced by a line heat source. Our first objective is to check experimentally the scale analysis performed in Duluc et al. (2003) and to provide detailed assessment of the numerical approach of transient free convection around a line source. In order to check the scaling laws in terms of heating power, three heat fluxes have been investigated experimentally and velocity fields have been measured by PIV techniques to confirm that the scaling laws proposed are valid for long time. As a limited computational domain is combined with artificial outer boundary conditions in numerical simulations, it becomes relevant and important to assess the validation of numerical results obtained for transient free convection. Part of the assessment has been done in Xin et al. (2004) and the second objective of the present work aims at a more refined assessment. One may *a priori* distinguish two different phases during the computation of external free convection in a limited domain. The first phase begins with the set-up of convection and ends when the fluid at the outer boundary is no longer motionless (*i.e.*, transient external convection extends to the boundary of computational domain); thereafter starts the second phase. It can be expected that numerical simulation may predict well the first phase of transient external convection but that accurate predictions during the second phase should be much more difficult. The present work indeed suggests a three-stage scenario and addresses the validity of numerical results for each stage.

In the next section, a description of the physical phenomena is recalled and a brief presentation of the experimental techniques and numerical methods employed is given. Experimental and numerical results obtained with various heating rates are then reported and discussed. A detailed comparison of our numerical results with the experimental data of Brodowicz and Kierkus (1966) is presented before concluding remarks will finally be given.

2. Physical problem and investigation techniques

In this section, we present the physical problem of interest, free convection around a line source, the experimental set-up and the mathematical formulation and numerical methods used.

2.1. Free convection induced by a line heat source

A line source can be created experimentally by a thin wire heated by Joule effect. A heating step is applied to the wire and the transient of free convection around a line source starts.

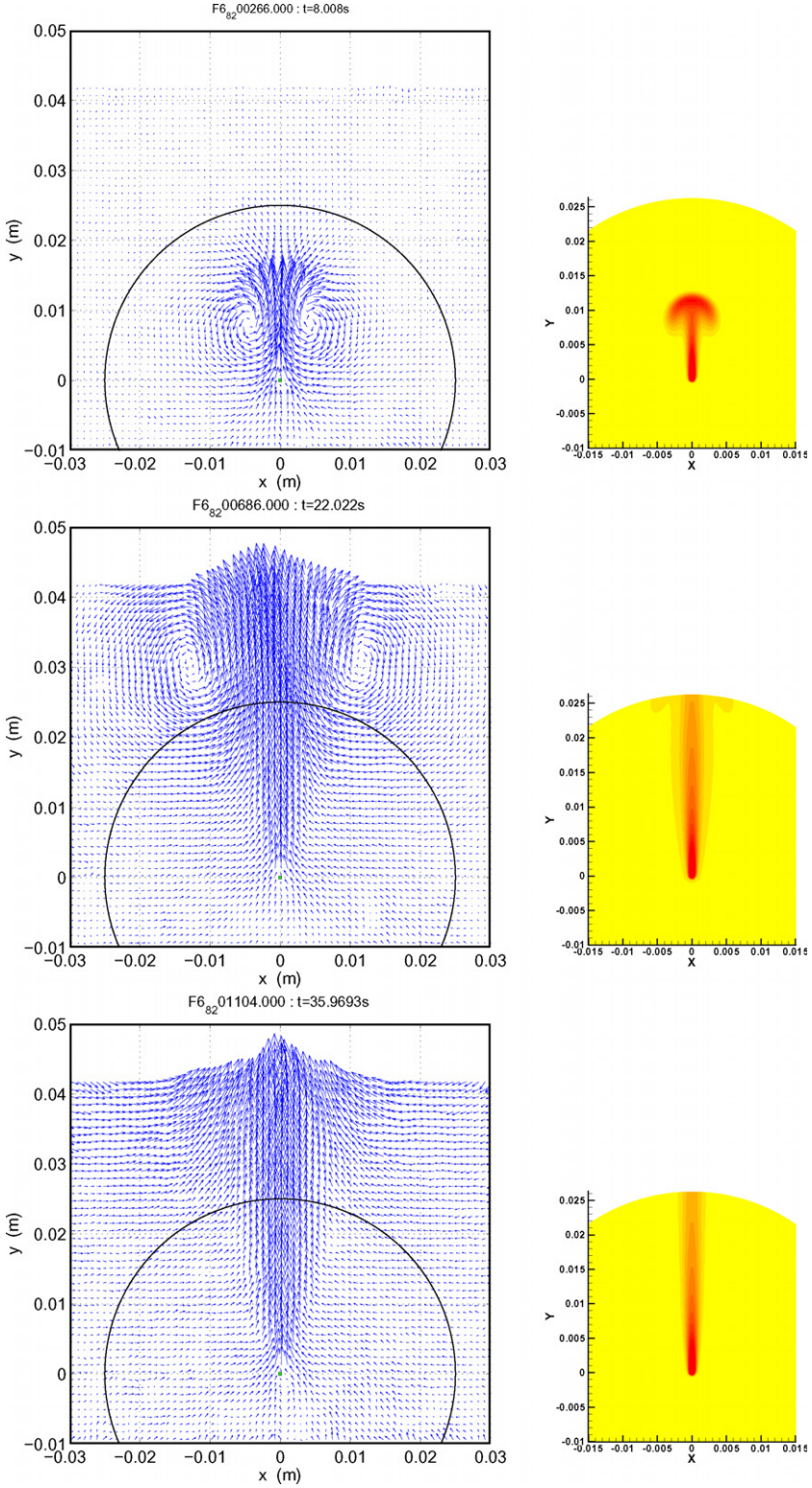

Fig. 1. Illustration of the three-stage scenario of transient external natural convection around a heated wire ($q_2 = 6.8 \times 10^4 \mathrm{W\,m^{-2}}$ and $R = 50\ \mu\mathrm{m}$). Velocity fields measured by PIV are displayed on the left and temperature fields obtained by numerical simulation on the right. The boundary of computational domain ($R' = 525R$) is shown as the black circle on the measured velocity fields.

Although end effects are unavoidable in an experimental set-up, free convection flow over the main part of the wire remains unaffected by the electrical supports. Comparison of experimental data measured in the wire vertical midplane with 2D numerical simulations is therefore relevant.

At early stages, heat is transferred from the wire to the surrounding fluid through molecular diffusion and the isotherms are concentric cylinders. After a time delay, one observes an upward fluid motion which results from the variation of fluid density induced by temperature increase. Isotherms are no longer concentric and evolve rapidly to a flame bulb shape first and then to a mushroom contour. The upward fluid motion induces two lateral symmetric circulations, the initial vortices, whose size increases with time. As an illustration, velocity vectors obtained experimentally from the PIV measurements and temperature fields derived from numerical simulations are presented in Fig. 1. Boundary of the computational domain is represented by the black arc on the velocity fields. On the numerical side, Fig. 1 shows that the transient process seen in the numerical simulation may be divided into three stages. Stage 1 starts at $t = 0$ and extends to the time t_1 over which both the main flow and temperature increase take place inside of the computational domain, *i.e.*, the flow field at the domain boundary is weakly perturbed by the initial vortices. Stage 2 corresponds to $t_1 < t < t_2$, during this stage the temperature front (the mushroom contour) and the two recirculations (the initial vortices) arrive at, cross and leave the boundary of the computational domain. Stage 3 corresponds to $t > t_2$. The temperature front and the two circulations have left the computational domain and the flow near the wire becomes stationary.

It is important to note that, for numerical simulations, this three-stage scenario always holds for transient external convection no matter how large the computation domain. However t_1 and t_2 are not intrinsic scales and depend strongly on the size of computation domain. This has already been shown in Xin et al. (2004) and is a fundamental issue of numerical modeling of external natural convection.

2.2. Experimental set-up

In the experimental set-up, the line heat source is a thin platinum wire heated by Joule effect. The thin wire is immersed horizontally in a large pool of demineralized water, the whole system being initially at room conditions. The platinum wire is 50 μm in radius (R) and 5 cm long. The pool is a rectangular cavity 20 cm wide, 40 cm long and 25 cm high. In order to limit temperature variation of the bath, the cavity is inserted into a bigger cavity 30 cm wide, 60 cm long and 34 cm high. The two containers are made of glass and filled up with demineralized water. The water free surface is about 15 cm above the wire. Photographs of the experimental set-up are displayed in Fig. 2.

Velocity fields are measured by PIV techniques. A vertical laser light sheet is located perpendicularly to the horizontal wire and midway between the wire ends in order to avoid end effects. Seeding is achieved by polyacid particles of 20 μm in diameter and 1.03 in density. A CCD camera with 8 bits resolution (768 × 484 pixels) is used. Each recording consists of a series of 600 pictures, the time delay between two neighboring frames being either 1/15 s or 1/30 s. The instantaneous 2D velocity field is obtained from a pair of neighboring frames by an original method based on optical flow algorithm rather than on the commonly used cross-correlation method Quénot et al. (1998). This method allows a finer spatial resolution of the velocity field (1 velocity vector per pixel) and is more robust against noise (Stanislas et al., 2005). It is invaluable in the present case as different spatial scales are involved: a good spatial resolution is required near the wire at early stages and also away from the wire at long time. The wire, heated by Joule effect, is connected to a power supply. The stepwise heating is performed using a relay of very short closing time (about 7 μs). The electrical circuit enables to realize heating steps of various magnitude and duration. In addition, a light emitting diode connected to the electrical circuit is positioned in the camera vision field. The diode is switched off by the relay when the step heating begins, which allows for the detection of the first image, *i.e.* the beginning of the transient, in the series of recorded frames.

Temperature measurements in the plume have also been carried out by using a K-type micro-thermocouple of 12.5 μm in diameter: the thermocouple is mounted on a two-dimensional positioner and a cathetometer is used to determine its horizontal and vertical locations with an accuracy of ±30 μm and ±10 μm respectively. Times series have been recorded with a sampling frequency of 128 Hz for about 20 s. The data acquisition system ensures a global accuracy on the temperature measurement better than ±0.15 K. We took care to minimize the influence of the temperature probe on the flow and thermal fields by limiting the use this technique to regions showing small temperature gradients, that is well above the wire ($\simeq 100R$). Furthermore as we are dealing with a very low Reynolds number laminar flow, one expects only a weak influence of the temperature probe. More details will be given in Section 3.1.4. Note also that the temperature probe was removed for velocity measurements.

The results reported in the present work are obtained for three different heat fluxes across the wire surface: $q_1 = (4.4 \pm 0.1) \times 10^4$ W m^{-2}, $q_2 = (6.8 \pm 0.1) \times 10^4$ W m^{-2} and $q_3 = (9.4 \pm 0.1) \times 10^4$ W m^{-2}. The corresponding volumetric powers of Joule effect can be calculated by $Q_v = 2q/R$. The corresponding values of the Rayleigh number (based on the heat flux) are equal to 0.01, 0.015 and 0.021, respectively.

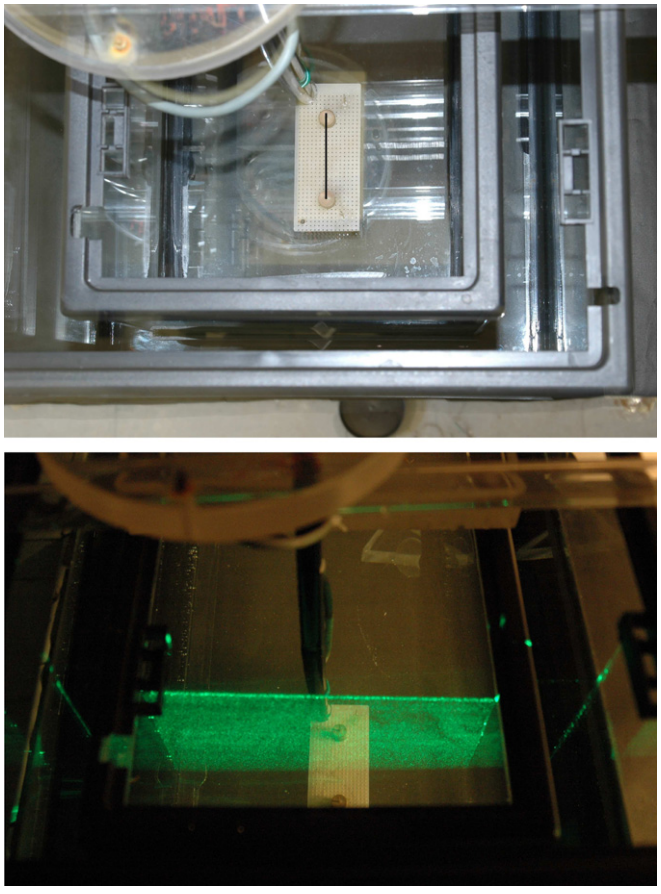

Fig. 2. Top view of the experimental set-up (top) and top-front view with laser sheet and seeding (bottom). The wire is too thin to be seen and it is drawn on its supports (top).

As far as are concerned the end effects, temperature distribution along the wire axis has been estimated under stationary conditions using a fin model (see Appendix A in Duluc et al. (2003)). The same model applied to the present experimental conditions shows that the end effects are of limited extension ($\leqslant 20\%$ of the wire length): temperature distribution along the wire axis is thus uniform at least over 80% of the wire length. As a consequence, the physical problem is essentially two-dimensional and the measurements have been merely performed in the wire midplane.

2.3. Mathematical formulation and numerical methods

2.3.1. Governing equations

In the numerical approach, the working fluid is considered as a Newtonian fluid of density ρ, volumetric expansion coefficient β, thermal diffusivity κ (thermal conductivity λ and specific heat C_p) and kinematic viscosity ν. The values of thermal–physical properties at ambient temperature T_0 are used. Fluid flow above and around the heating wire is assumed to be two-dimensional and governed by the following Navier–Stokes equations in polar coordinates:

$$\begin{cases} \frac{\partial u}{\partial r}+\frac{u}{r}+\frac{1}{r}\frac{\partial v}{\partial \theta}=0 \\ \frac{\partial u}{\partial t}+u\frac{\partial u}{\partial r}+\frac{v}{r}\frac{\partial u}{\partial \theta}-\frac{v^2}{r}=-\frac{1}{\rho}\frac{\partial p}{\partial r} \\ \quad +\nu\left[\left(\frac{\partial^2}{\partial r^2}+\frac{1}{r}\frac{\partial}{\partial r}-\frac{1}{r^2}+\frac{1}{r^2}\frac{\partial^2}{\partial \theta^2}\right)u-\frac{2}{r^2}\frac{\partial v}{\partial \theta}\right] \\ \quad -g\beta(T-T_0)\cos(\theta) \\ \frac{\partial v}{\partial t}+u\frac{\partial v}{\partial r}+\frac{v}{r}\frac{\partial v}{\partial \theta}+\frac{uv}{r}=-\frac{1}{\rho r}\frac{\partial p}{\partial \theta} \\ \quad +\nu\left[\left(\frac{\partial^2}{\partial r^2}+\frac{1}{r}\frac{\partial}{\partial r}-\frac{1}{r^2}+\frac{1}{r^2}\frac{\partial^2}{\partial \theta^2}\right)v+\frac{2}{r^2}\frac{\partial u}{\partial \theta}\right] \\ \quad +g\beta(T-T_0)\sin(\theta) \\ \frac{\partial T}{\partial t}+u\frac{\partial T}{\partial r}+\frac{v}{r}\frac{\partial T}{\partial \theta}=\kappa\left(\frac{\partial^2}{\partial r^2}+\frac{1}{r}\frac{\partial}{\partial r}+\frac{1}{r^2}\frac{\partial^2}{\partial \theta^2}\right)T \end{cases} \quad (1)$$

where t is the time, u and v are the radial and azimuthal velocity components, p is the pressure deviation from the hydrostatic pressure, g is the gravitational acceleration and T is the temperature.

In order to study the effects of wire's thermal inertia on the transient, Eqs. (1) are coupled with the heat conduction equation in the wire:

$$\widetilde{\rho}\widetilde{C}\frac{\partial T}{\partial t}=\widetilde{\lambda}\left(\frac{\partial^2}{\partial r^2}+\frac{1}{r}\frac{\partial}{\partial r}+\frac{1}{r^2}\frac{\partial^2}{\partial \theta^2}\right)T+Q_v \quad (2)$$

where $\widetilde{\rho}$, $\widetilde{C}$ and $\widetilde{\lambda}$ are respectively the wire's density, specific heat and thermal conductivity and Q_v is a uniform heat source induced by Joule effect. Heat flux conservation is applied across the wire surface: $\lambda\frac{\partial T}{\partial r}|_{\text{fluid}}=\widetilde{\lambda}\frac{\partial T}{\partial r}|_{\text{wire}}$ at $r=R$ where R is the wire's radius. The Biot number defined as $Bi\equiv hR/\widetilde{\lambda}$ may be computed considering a typical value for the heat transfer coefficient equal to 5000 W m^{-2} K^{-1}. The thermal conductivity of platinum is about 72 W m^{-1} K^{-1} and the wire radius is equal to 50 μm. One obtains a Biot number largely smaller than 0.1. Thus, the wire is almost at a uniform temperature. Note that velocity components are defined on $(r,\theta)\in[R,R']\times[0,2\pi]$ while the temperature field is defined on $(r,\theta)\in[0,R']\times[0,2\pi]$.

2.3.2. Boundary and initial conditions

As we are interested in transient free convection, the initial condition is motionless fluid at ambient temperature T_0. The superheat, $\Delta T=T-T_0$, is usually used to characterize temperature field.

The wire surface $(r=R)$ is assumed to be impervious and no-slip. At the external boundary of the computational domain $(r=R'\gg R)$, we imposed $\frac{\partial T}{\partial r}=0$ for temperature and the following boundary conditions for velocity–pressure coupling:

$$\begin{cases} v\left(\frac{\partial}{\partial r}+\frac{1}{r}\right)u=\frac{p}{\rho} \\ v\left(\frac{\partial}{\partial r}+\frac{1}{r}\right)v=0 \end{cases} \quad (3)$$

Conditions (3) are derived from a pressure and friction balance and the assumption that all angular derivatives are negligibly small compared to radial ones. More details about the boundary conditions and their numerical implementation can be found in Duluc et al. (2003), Xin et al. (2004).

2.3.3. Numerical methods

Eqs. (1) and (2) are discretized in time by a second order scheme of finite difference type: for stability reasons the diffusion terms are treated implicitly while convective terms are treated explicitly. The spatial approximation makes use of basis functions made of tensor products of Chebyshev polynomials and Fourier series due to the periodicity in the azimuthal direction, see for instance Canuto et al. (1988), Bernardi and Maday (1992). In order to obtain adapted mesh distribution, a domain decomposition technique (Smith et al., 1996) is used in radial direction. The domain $[R,R']$ is divided into several subdomains and over each subdomain a Chebyshev collocation method and a Fourier Galerkin method are used. Continuity of both functions and their first radial derivatives at the subdomain interfaces is imposed by means of Schur complement. The velocity–pressure coupling is enforced by standard projection method making use of time-splitting (Guermond and Quartapelle, 1998). More details on the numerical algorithm and on the relevant numerical techniques can be found in Xin et al. (2004).

3. Results and discussion

In this section, we address, respectively, the transient and steady issues of free convection around a line source. We first discuss the transient free convection induced by a platinum wire heated by Joule effect and immersed in demineralized water and then comment on the steady case of free convection created by a thin wire in air heated by Joule effect.

3.1. Transient free convection

A stepwise heating is applied to the platinum wire immersed in demineralized water and the corresponding transient of free convection is investigated by both the experimental and numerical means. The ambient temperature in water, T_0, is equal to 293 K. Numerical studies are performed by choosing a limited computational domain, the artificial boundary conditions (3) and water thermophysical properties at T_0. Experimental measurements are realized in order to qualify and validate the numerical approaches.

Numerical simulations have been performed by using the following parameters: $R=5\times10^{-5}$ m and $R'=697R$. The domain $[R,R']$ is divided into 11 subdomains of increasing size and each subdomain is discretized by 31 Chebyshev collocation points. In the azimuthal direction 90 Fourier modes are used. It is important to note that $R'=697R\approx0.035$ m is larger than the computational domain shown in Fig. 1.

3.1.1. Scaling laws

Before commenting on the results obtained for different heating rates, it is useful to recall the characteristic scales associated to the onset of convective motion around a line source induced by a stepwise heating. Concerning the convection onset, the fluid superheat, ΔT, the extension of non isothermal zone, δr, the fluid velocity of convective motion, v, and the characteristic time for convection onset, t, are linked to the heat flux, q, and other quantities as follows:

$$\delta r\sim\left(\frac{\lambda\nu\kappa}{g\beta q}\right)^{1/4},\quad t\sim\sqrt{\frac{\lambda\nu}{\kappa g\beta q}},\quad v\sim\kappa\left(\frac{g\beta q}{\lambda\nu\kappa}\right)^{1/4},\quad \Delta T\sim\frac{q}{\lambda}\left(\frac{\lambda\nu\kappa}{g\beta q}\right)^{1/4}$$

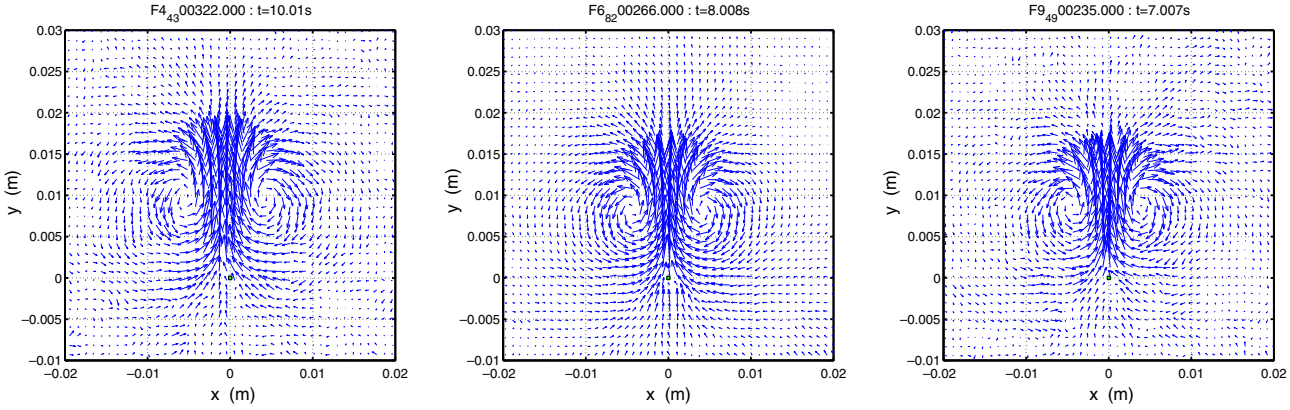

Fig. 3. Velocity fields measured by PIV at $tq^{1/2} = 21$. The corresponding times are respectively equal to 10 s for q_1 (left), ≈8 s for q_2 (middle) and ≈7 s for q_3 (right).

These scaling laws are presented in terms of the heat flux q which is the governing parameter in experiments. It is important to keep in mind that the characteristic velocity of convective motion scales as $q^{1/4}$ and the characteristic time as $q^{-1/2}$. This scaling analysis was developed in a previous work (Duluc et al., 2003) and confirmed by the numerical simulations. In addition, it was also revealed that the long time behavior of the transients was also adequately characterized by $t \sim q^{-1/2}$. As the same scaling of $t \sim q^{-1/2}$ also characterizes the convection onset, what is meant here by 'long time' is the time for which flow and temperature fields near the wire surface become almost stationary while the flow and temperature fields away from the wire may still strongly evolve.

If the scaling of $t \sim q^{-1/2}$ holds for velocity fields at long time, similar flow structure should be observed for equal values of $tq^{1/2}$. Fig. 3 displays the measured velocity fields corresponding to $tq^{1/2} = 21$ for the three different heating rates investigated. The corresponding physical times are listed in Table 1. As can be observed from Fig. 3, the velocity fields are in very good qualitative agreement in that the two initial vortices have the same spatial extension and their centers are located at the same vertical position. It can be concluded that at least the scaling of $t \sim q^{-1/2}$ holds qualitatively up to this particular value of $tq^{1/2} = 21$. It is noted that, given the fact that the computational domain extends to $R' = 0.035$ m, at $tq^{1/2} = 21$ the two initial vortices are still within the computational domain and the flow fields displayed in Fig. 3 still belong to the first stage. The measured velocity fields at $tq^{1/2} = 42$ are shown in Fig. 4 and the same qualitative agreement is also observed.

Table 1
Real time corresponding to constant values of $tq^{1/2}$ for the three heat fluxes studied

$tq^{1/2}$	q_1	q_2	q_3
21	10 s	≈8 s	≈7 s
42	20 s	≈16 s	≈14 s

$q_1 = 4.4 \times 10^4$ W m^{-2}, $q_2 = 6.8 \times 10^4$ W m^{-2} and $q_3 = 9.4 \times 10^4$W m^{-2}.

Fig. 5 displays quantitative comparisons between measurements and numerical results for the vertical velocity component on the symmetry axis for two values of $tq^{1/2}$, 21 and 42. The figures show that the computed velocity profiles are in good agreement with the experimental measurements. Note that the experimental curves display a noisy aspect. This is due to the fact that the weak velocity in the transient process leads any small perturbation to become important and visible on the measured results.

At $tq^{1/2} = 21$, the vertical velocity increases rapidly from zero on the wire surface to a maximum value at $y \approx 0.0075$ m and then decreases to zero at $y \approx 0.025$ m. At $tq^{1/2} = 42$, the location of maximum vertical velocity occurs $y \approx 0.02$ m and at the domain boundary ($y = R' = 0.035$ m) vertical velocity becomes important. This means that $tq^{1/2} = 42$ belongs to the end of the first stage as the centers of the two vortices and the temperature front are located at $y \approx 0.02$ m and are about to reach, cross and leave the domain boundary. The overall observation is that at constant $tq^{1/2}$, vertical velocity profiles display similar form and especially for different heating rates the maxima of vertical velocity occur almost at the same vertical position. Despite the slight discrepancy between the y values at which the vertical velocity maxima occur, it can be concluded that during the transients of free convection around a

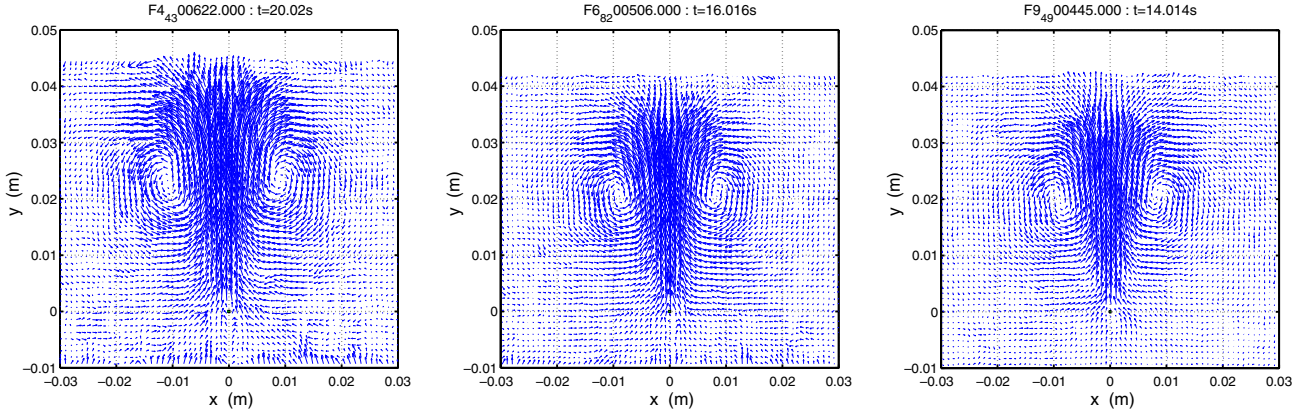

Fig. 4. Velocity fields measured by PIV at $tq^{1/2} = 42$. The corresponding times are respectively equal to 20 s for q_1 (left), ≈ 16 s for q_2 (middle) and ≈ 14 s for q_3 (right).

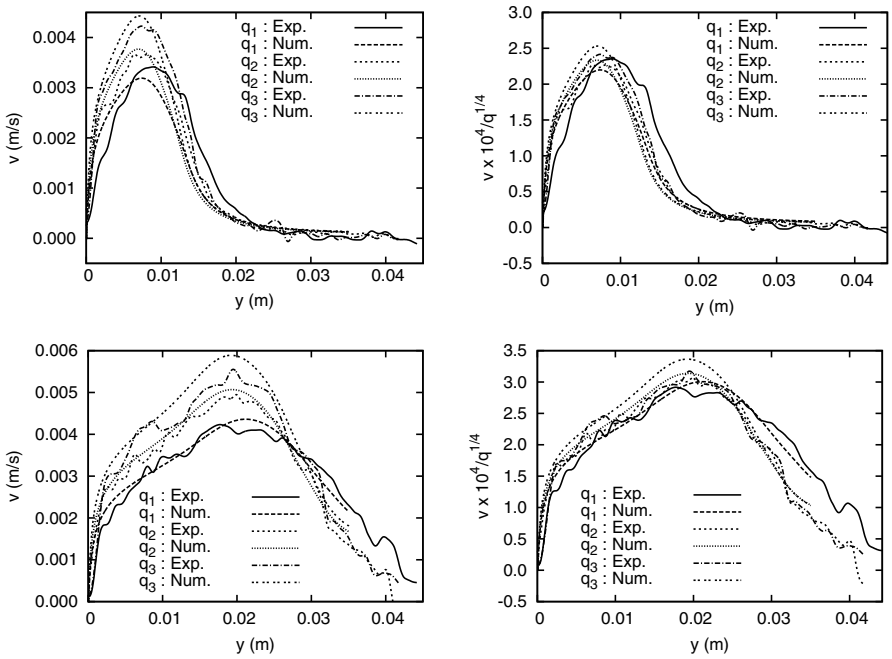

Fig. 5. Vertical velocity profiles above the wire at $tq^{1/2} = 21$ (top left) and 42 (bottom left). Same plots with velocity rescaled by $q^{1/4}$ (top right and bottom right).

line source the positions of maximal vertical velocity and centers of initial vortices scale as $q^{-1/2}$.

It is also observed from Fig. 5 that at constant $tq^{1/2}$ higher heating rate results in a stronger velocity of convective motion. As scaling analysis performed suggest that vertical velocity is proportional to $q^{1/4}$, the rescaled velocity profiles are also displayed in Fig. 5. Although the scattering is much less, they however do not collapse completely, which suggests that the $q^{1/4}$ velocity scaling is good but not completely satisfactory. As the scalings of $t \sim q^{-1/2}$ and $v \sim q^{1/4}$ have been established only for the onset of convective motion induced by a stepwise heating of a thin wire, it is quite unexpected and outstanding that these scalings remain meaningful and to some extend appropriate for characterizing the long time behavior of transient free convection around a line source.

3.1.2. Detailed comparison of velocity profiles

In this section a more detailed comparison between experimental and numerical results is performed, looking at profiles of vertical velocity, v, and horizontal velocity, u, at several heights above the wire. Due to the similarity between the solutions obtained at different heating rates we chose to perform the comparisons for q_2 only. For completeness comparison is performed at each stage of the three-stage scenario proposed above, aiming at validating the numerical simulations stage by stage.

3.1.2.1. Stage 1. Fig. 6 displays profiles of vertical velocity and horizontal velocity at $t = 8$ s ($tq^{1/2} \approx 21$) and confirms the good agreement between experimental and numerical results, which is observed from Fig. 5. Above the wire, vertical velocity remains positive and convective flow is upwards ($v > 0$). Outside of the region of upward motion, there is a slight downward flow ($v < 0$) which is

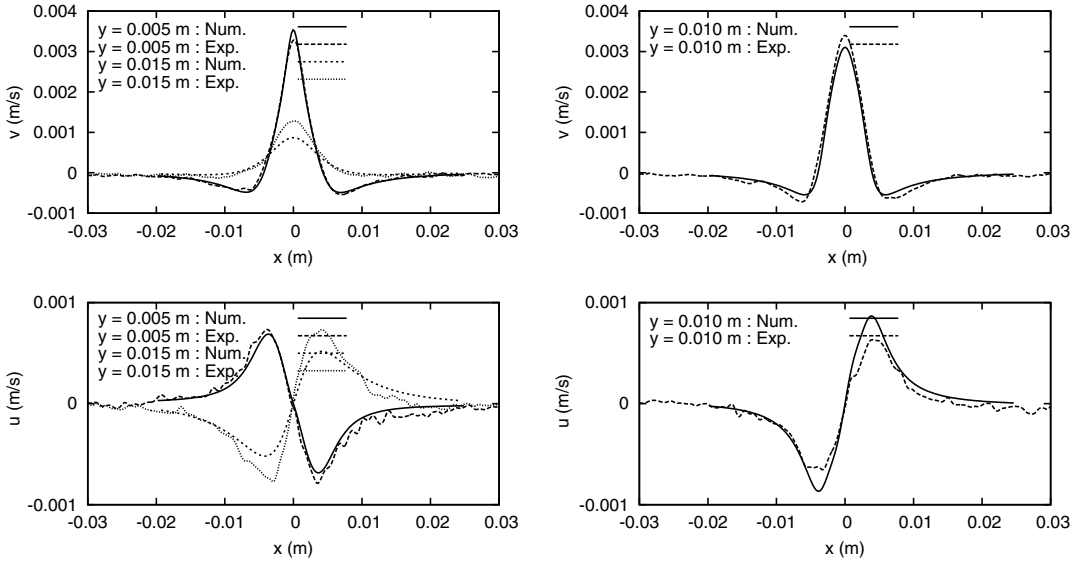

Fig. 6. Profiles of vertical velocity, v (top) and horizontal velocity, u (bottom) above the wire obtained for q_2 at $t = 8$ s.

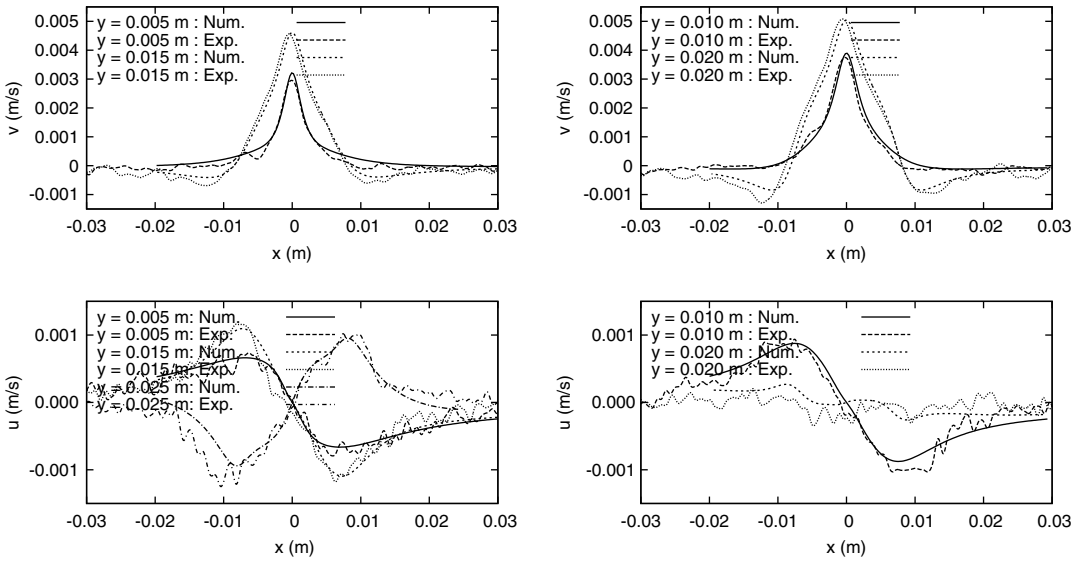

Fig. 7. Profiles of vertical velocity, v (top) and horizontal velocity, u (bottom) above the wire obtained for q_2 at $t = 16$ s.

associated to the two initial vortices: the most important downward flow is observed for $x \approx \pm 0.006$ m at $y = 0.005$ m and 0.01 m. At $y = 0.005$ m, u velocity is positive for $x < 0$ and negative for $x > 0$ while at $y = 0.01$ m and 0.015 m it is negative for $x < 0$ and positive for $x > 0$. This agrees with the observation from Figs. 1 and 4 that the centers of the vortices are located between $y = 0.005$ m and $y = 0.01$ m. As at $t = 8$ s the two vortices extend to $y = 0.015$ m above the wire at $x = 0$, fluid motion is weak at higher y positions and no profiles are shown for larger y values.

Fig. 7 details velocity profiles at $t = 16$ s ($tq^{1/2} \approx 42$). The two initial vortices extend toward the domain boundary and their centers are located at $y \approx 0.020$ m. Downward flow occurs therefore at $x \approx \pm 0.011$ m for $y = 0.015$ m and 0.02 m and no downward flow is observed for $y = 0.005$ m and 0.01 m. As the centers of the vortices are located at $y \approx 0.02$ m, the most important downward flow occurs at $y = 0.02$ m and the corresponding u velocity is very weak: for smaller y, u velocity is positive for $x < 0$ and negative for $x > 0$ and for $y = 0.025$ m it is negative for $x < 0$ and positive for $x > 0$. The overall observation is that numerical results are in good agreement with the experiment.

Owing to the good agreement between the experimental and numerical results, it is concluded that, during the first stage of transient free convection, the numerical simulations reproduce very closely the physical phenomena. One can, therefore, rely on the numerical approach proposed to predict Stage 1 of transient free convection.

3.1.2.2. Stage 2. The characteristic field of the second stage displayed in Fig. 1 corresponds to $t = 22$ s and $q_2 = 6.8 \times 10^4$ W m^{-2}. At this time, the two vortices cross the domain boundary located at $R' = 0.035$ m and their centers are located just inside of the domain boundary. Fig. 8 illustrates the corresponding horizontal and vertical velocity profiles. As can be seen, the agreement between the experiment and numerical simulation remains good for $y = 0.01$ m and 0.02 m and it becomes worse for $y = 0.03$ m. This is characteristic of what happens during the second stage: numerical investigation predicts correctly flow structure and flow scales in the region away from the domain boundary but it displays more discrepancy in the region around the plume outlet and near the domain boundary. This larger difference is mainly due to the artificial boundary conditions which cannot be expected to be fully satisfying.

We can nevertheless conclude that away from the domain boundary the numerical results are in good agreement with the experiment, *i.e.*, with the physical phenomena, when the initial vortices are arriving at, crossing and leaving the domain boundary. One can, therefore, expect a reasonable prediction of near-field during Stage 2.

3.1.2.3. Stage 3. In a previous study (Xin et al., 2004), it was concluded that, based on the vertical velocity profiles, at long time after the vortices have left the computational domain, agreement between numerical simulation and experimental investigation was observed everywhere in the computational domain. In order to refine this conclusion, we display in Fig. 9 the long time behavior of numerical results in comparison with experimental data. Fig. 9 shows that it is not exact to say that, at long time, agreement between numerical simulation and experimental investigation can be observed everywhere in the computation domain and that it is more exact to say the following: for $r < R'/3$ full agreement is observed apart from spurious values in u velocity measurements; for $r > R'/3$ agreement is observed only in the main stream of the thermal plume. Outside of the main stream, one observes on both u and v velocities a slight discrepancy which can be certainly neglected in comparison with the main stream velocity. But note that, due to the boundary conditions used, numerical results display a slight downward flow which does not exist at all in the experiment. This means that the current boundary conditions are not completely compatible with far flow field and that in the future more efforts are needed on mathematical modeling of the boundary conditions for free convection flows.

3.1.3. Trajectory of the vortex center

In our previous study (Xin et al., 2004), it was shown that the centers of the initial vortices evolve in time along a linear trajectory. Fig. 10 displays the trajectories of the vortex center obtained for the three heating rates. One observes first of all that the trajectory of vortex center is independent of heating rate. Although numerical results show a slight difference in the trajectory and experimental data are scattered, an approximate agreement between numerical and experimental results is observed.

The scattering of experimental measurements is due to the fact that velocity scales of $\mathcal{O}$ (mm/s) are very small and that the experimental noise is at the level of u velocity as is shown by Figs. 6–9.

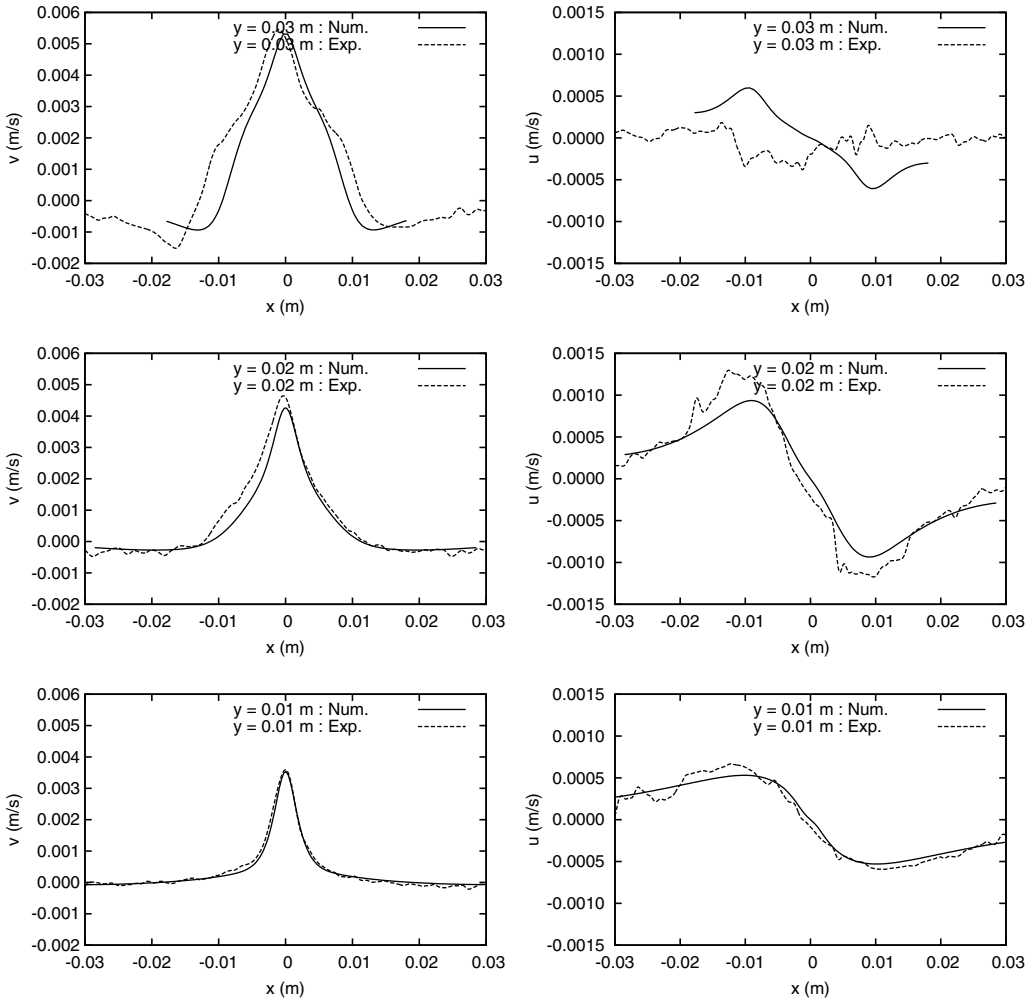

Fig. 8. Profiles of vertical velocity, v (left) and horizontal velocity, u (right) above the wire obtained for q_2 at $t = 22$ s.

The vortex center computed from the scattered experimental data exhibits also a scattering feature. Note that, when the initial vortices arrive at and cross the domain boundary, the trajectory predicted by numerical simulation is deviated from the linear path that the vortex center should follow in the case of a larger computational domain. This may explain why during stage 2 more discrepancy between numerical simulation and experiment is observed around the thermal plume near the domain boundary. This also suggests that, as far as is concerned the vortex center, the agreement between numerical and experimental results can only be observed during stage 1.

Based on the experimental data, an analytical law can be established for the trajectory of the vortex center: for the left vortex its center evolves as $y = -2.5 \times (x + 0.001)$ and for the right one its center evolves as $y = 2.5 \times (x - 0.001)$ with x and y in the unit of meter. This yields the vertical position of -0.0025 m for the virtual line source. These laws for the trajectory, as well as the trajectories shown in Fig. 10, do not involve time scale with which the vortex center arrives at a particular position. For the position of $y \approx 0.02$m, for example, the vortex center crosses this position at approximately 20 s for q_1, 16 s for q_2 and 14 s for q_3.

3.1.4. Temperature profile

We worked with a superheat $T - T_0$ less than 15 K on the wire surface in order to stay within the validity of Boussinesq assumption. Temperature increases only slightly in the working fluid which is demineralized water. For temperature measurements the highest heating rate, q_3, was used so as to get significant temperature increase at least at the position of $y = 0.005$ m.

After the micro-thermocouple of 12.5 μm is moved to a desired position and before a heating step is supplied to the wire, we record on a data acquisition board both the e.m.f. of the thermocouple and the voltage supplied to the wire. This allows detecting on the thermocouple signal the beginning of the heating step. Fig. 11 depicts the time evolution of temperature at $x = 0$ and $y = 0.005$ m. After a time delay, the plume front (the head of mushroom) reaches the position of the micro-thermocouple: temperature first rises rapidly to a maximum, then decreases slowly to a minimum and finally increases extremely slowly to a constant value. In the experiment, the maximum value is lower than the numerical one and there is furthermore a small time delay. Both features result from the thermal mass effects associated with the probe. Time constant of the micro-thermocouple is estimated to be about 0.001 s. This value is however still too high to achieve accurate measurements of the fastest physical events. Apart from the maximum value and the time delay, a good agreement is observed between numerical and experimental results during the whole transient.

Fig. 12 displays temperature profile of quasi-steady state at $y = 0.005$ m. As is illustrated, the maximal temperature increase is only equal to approximately 1.5 K and remains very small indeed. Despite the weak temperature increase, numerical results agree well with temperature measurements.

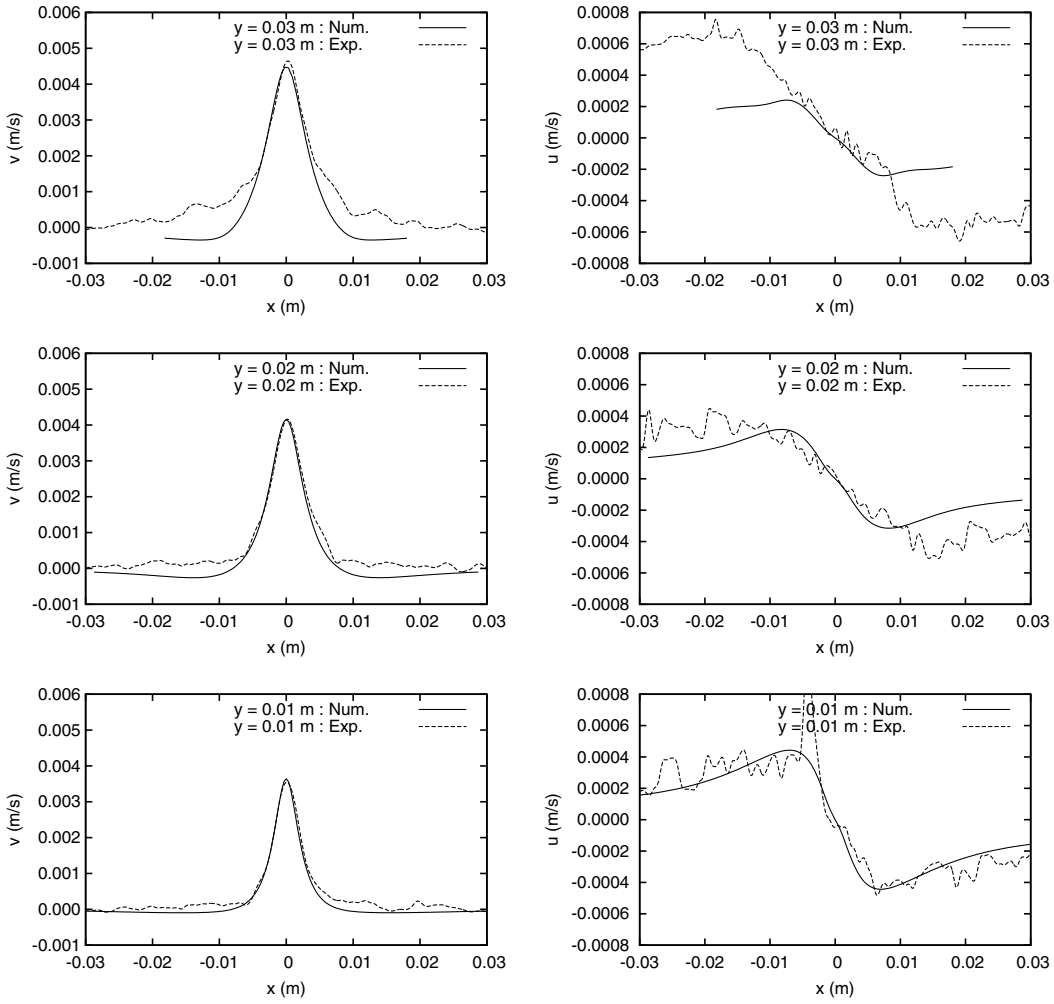

Fig. 9. Profiles of vertical velocity, v (left) and horizontal velocity, u (right) above the wire obtained for q_2 at $t = 38$ s.

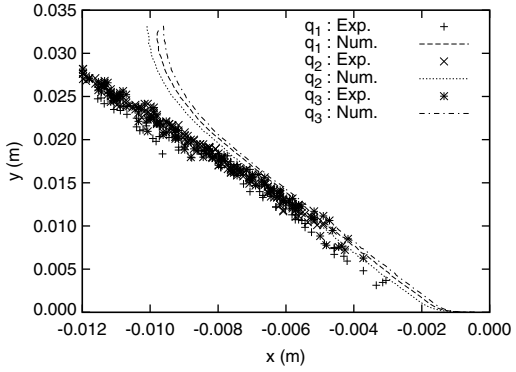

Fig. 10. Physical trajectories of the initial vortex center measured for the three heating rates, q_1, q_2 and q_3.

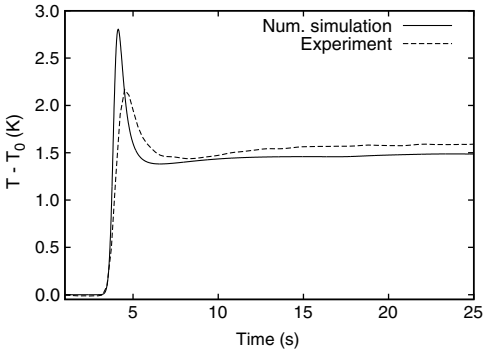

Fig. 11. Time evolution of temperature at $x = 0$ and $y = 0.005$ m for heating rate q_3.

The temperature probe is a small element inserted in the flow. The corresponding Biot number can be estimated in the same way as for the wire using the following properties: thermocouple dimension of 6.25 μm, heat transfer coefficient $h \sim 5000\ \mathrm{W\,m^{-2}\,K^{-1}}$ and thermal conductivity of chromel or alumel alloys of $\sim 20\ \mathrm{W\,m^{-1}\,K^{-1}}$ and a value well below 0.1 is obtained. The thermocouple acts therefore as an isothermal metallic inclusion whose typical dimension is 12.5 μm. In order to estimate the effect of the temperature probe on the flow under stationary conditions, one has to examine the temperature difference that would be present in the absence of the probe. First considering the x direction, one can see from Fig. 12 that the temperature gradient is about 1 K/mm. The temperature difference over 12.5 μm is thus lower than 0.02 K. In the y direction, the thermocouple is located well above the wire ($y = 0.005\ m = 100R$) where the temperature gradient in the vertical direction is weak (Xin et al., 2004). Lastly, temperature is uniform in the z direction (2D configuration). Then for all directions, the temperature

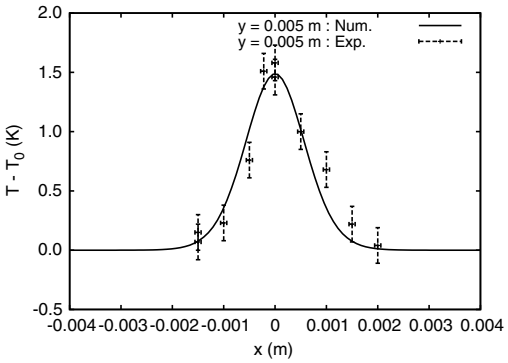

Fig. 12. Temperature profile at quasi-steady state at $y = 0.005$ m for heating rate q_3.

difference to be measured is equal or close to zero. This value is similar with the one imposed by the thermocouple. The physical temperature field is thus slightly modified by the temperature probe.

3.2. Steady free convection

Although Fig. 9 displays results of steady free convection, a challenging comparison should be done with the independent experimental study realized by Brodowicz and Kierkus (1966): a thin metal wire 37.5 μm in radius is placed horizontally in air and heated by Joule effect. The ambient temperature in air, T_0, is equal to 293 K. The applied heating power per volume, Q_v, is equal to 2.2069×10^9 W m^{-3}, it is equivalent to a heat flux of 4.138×10^4 W m^{-2} and a heat supply of 9.75 W m^{-1} applied to the wire surface. Temperature and velocity profiles have been measured at various heights above the wire.

In the numerical approach, $R = 3.75 \times 10^{-5}$ m and $R' = 1865R$. The domain $[R, R']$ is divided into 17 subdomains and each subdomain is discretized by 31 Chebyshev collocation points. In the azimuthal direction, 170 Fourier modes are used. The thermophysical properties of air at $T_0 = 293$ K are chosen for computing Rayleigh number and other parameters. Since the wire material was not specified in Brodowicz and Kierkus (1966), we supposed that it was made of platinum: this assumption slightly modifies the transient but does not influence the flow structure at long time.

The numerical simulation performed under Boussinesq assumption reveals a wire superheat of 210 K which is far beyond the validity of Boussinesq assumption. Bearing this in mind, comparison between numerical results obtained under Boussinesq assumption and experimental data aims only at showing the qualitative agreement between them and confirming that we are able to obtain reasonable numerical results for free convection around a line heat source.

Flow structure measured in the experiment (Brodowicz and Kierkus, 1966) and obtained by the current numerical simulation is shown in Fig. 13. Well above the wire, dust trajectories show that: air flows horizontally from far away to the symmetry line at $x = 0$ and turns continuously upwards till the symmetry line; at the wire level and lower levels air is drawn from far away to the wire. Apart from a slight asymmetry under the wire, the experimental study reveals a symmetric flow. Numerical simulation predicts well the symmetric flow, but outside of the plume main stream there is a weak downward flow which is not really physical. This behavior, also observed from numerical solutions for long time transient flows (Fig. 9), is likely due to the imposed boundary conditions. Note nevertheless that below $y = 0.015$ m flow structure predicted by numerical simulation seems to agree well with the experimental visualization.

3.2.1. Velocity profiles

Velocity profiles at three vertical positions ($y = 0.01$ m, 0.02 m and 0.04 m) are shown in Fig. 14. Given that numerical simulation is performed under Boussinesq assumption and the wire's superheat is equal to 210 K, the agreement between numerical and experimental data should be considered as very good. As indicated above, a slight discrepancy is observed outside of the plume main

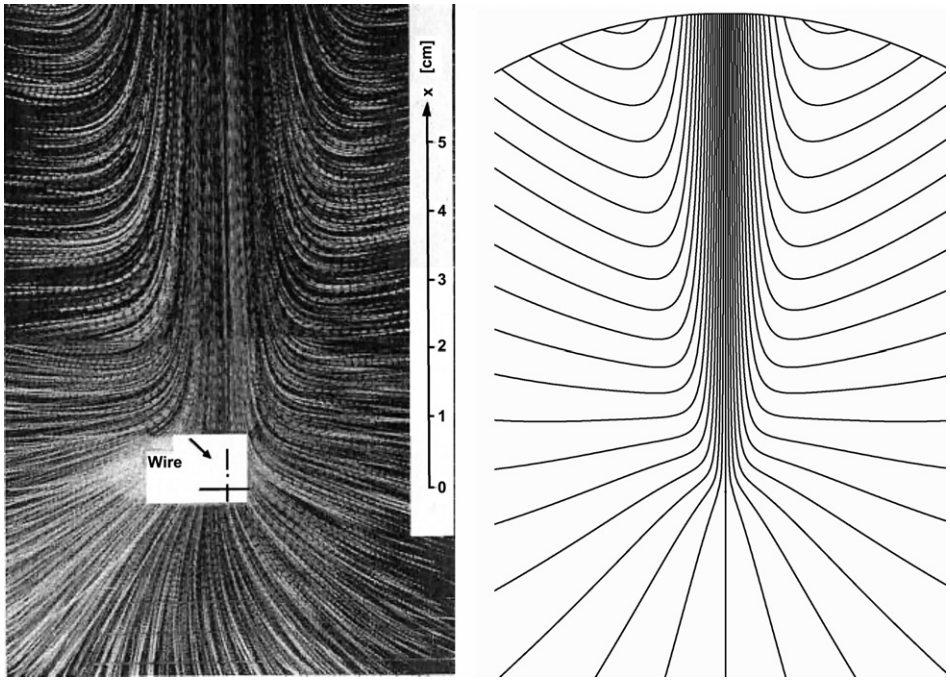

Fig. 13. Streamlines—dust trajectories (experiment, left) (Brodowicz and Kierkus, 1966) and stream function (numerical simulation, right) around and above the wire heated in air. The arc drawn on the stream function (right) corresponds to the domain boundary.

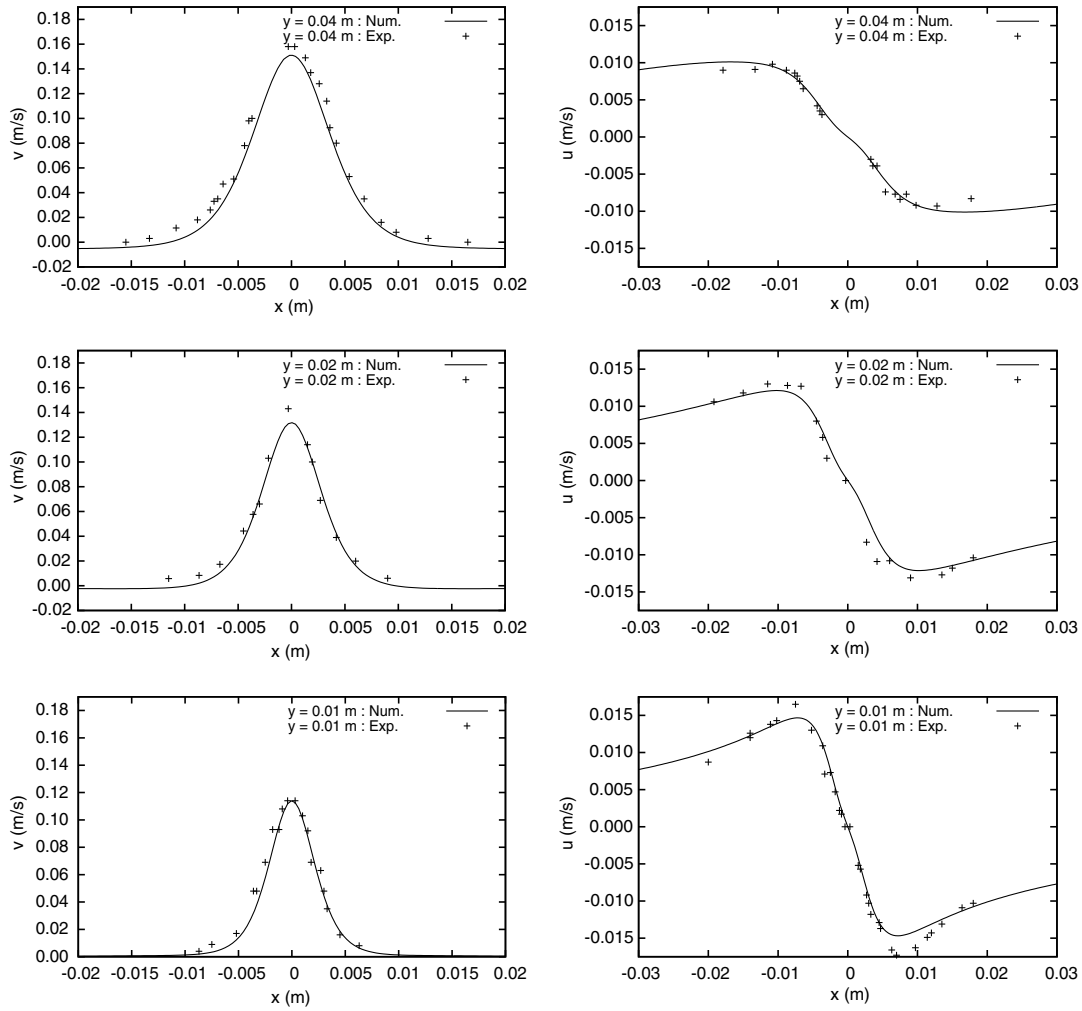

Fig. 14. Profiles of vertical velocity (left) and horizontal velocity (right) above the heated wire in air. Although the numerical simulation performed under Boussinesq assumption shows a wire superheat equal to 210 K, good agreement is found with experimental data despite a slight discrepancy observed about $x = 0$ at $y = 0.02$ m and 0.04 m.

stream at $y = 0.02$ m and 0.04 m due to the weak downward flow motion induced by the boundary conditions used. Note also that about $x = 0$ there is a small difference in v velocity at $y = 0.02$ m and 0.04 m.

3.2.2. Temperature profiles

Fig. 15 depicts temperature profiles at $y = 0.01$ m and 0.04 m. Numerical results are in good agreement with experimental measurements almost everywhere except for about $x = 0$ where a difference of approximately 10% is noticed for both temperature and velocity profiles. This discrepancy is likely to be due to the use of Boussinesq assumption in the numerical investigation. Indeed, in the experiment performed by Brodowicz and Kierkus, the wire superheat is about 210 K resulting in a significant increase of air temperature and corresponding variations of thermophysical fluid properties. Density decreases while values for viscosity (dynamic and kinematic), thermal conductivity or diffusivity increase with temperature. A more detailed numerical study including temperature dependence of the fluid properties should be usefully developed to check this assumption. One should note that these

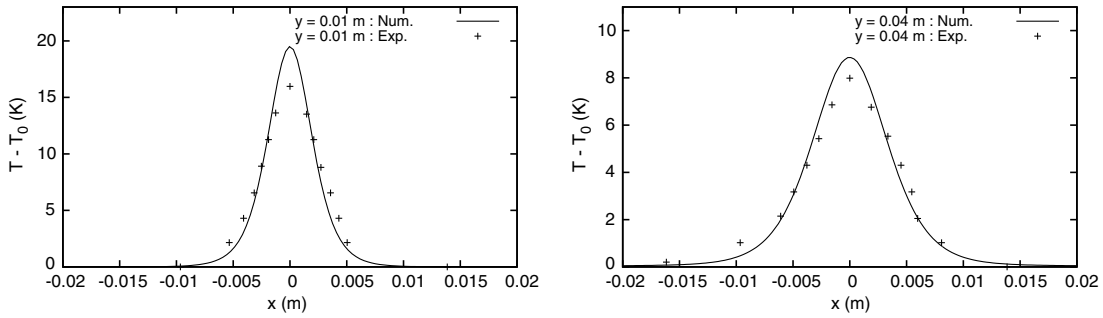

Fig. 15. Temperature profiles above the heated wire in air. Good agreement between experimental and numerical results is observed except near $x = 0$.

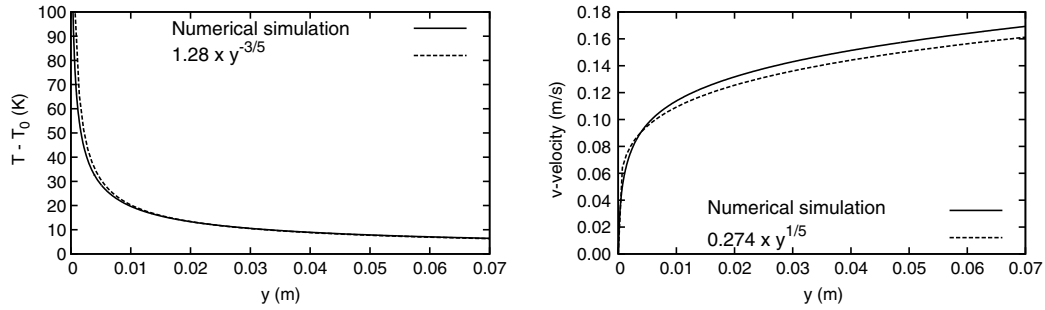

Fig. 16. Temperature (left) and vertical velocity (right) profiles above the heated wire in the symmetry line ($x = 0$). Similarity solutions ($T(y) - T_0 = 1.28y^{-3/5}$ and $v(y) = 0.274y^{1/5}$) are also plotted. A good agreement is observed for temperature distribution although a slight discrepancy is observed for vertical velocity.

effects are generally less important when dealing with a liquid. Indeed previously discussed experiments performed with water and corresponding to a wire superheat less than 15 K showed a much better agreement on the symmetry line $x = 0$.

Another possible reason for the discrepancy may be the measurement uncertainty in the experimental study of Brodowicz and Kierkus (1966). Unfortunately no error bars have been specified in their study. The conclusion that can be drawn from the comparison with their study (Brodowicz and Kierkus, 1966) stays mainly qualitative: the current numerical approach is able to yield the correct flow structure and the correct scales of velocity and temperature fields, especially in the near region around the wire.

3.2.3. Scaling laws and similarity solutions

In the far-field above the wire ($r >> R$ or $y >> R$), the horizontal extension of the thermal plume, δx, is small compared with y and boundary layer theory can be applied. Assuming $\delta x \sim y^m$, $v \sim y^n$ and $T - T_0 \sim y^l$, conduction–convection balance in the energy equation yields $2m + n = 1$, friction–buoyancy balancing yields to $l + 2m - n = 0$ and finally energy conservation in y direction, *i.e.* $\int_{-\infty}^{\infty} v(T - T_0)\mathrm{d}x = \text{constant}$, yields $l + m + n = 0$. This leads to $l = -3/5$, $m = 2/5$ and $n = 1/5$ and the following scales:

$$\delta x \sim y^{2/5} \quad v \sim y^{1/5} \quad T - T_0 \sim y^{-3/5}$$

These scales are recovered by most of similarity solutions. Gebhart et al. (1970) for example provided for $Pr = 0.7$ the following solutions on the symmetry line ($x = 0$):

$$T(y) - T_0 = \left(\frac{(2\pi Rq)^4\kappa^2}{64g\beta(1.245\lambda)^4Pr^2}\right)^{1/5} y^{-3/5}$$

$$\mathrm{v}(y) = 0.6618\left(\frac{4\kappa(g\beta 2\pi Rq)^2}{Pr(1.245\lambda)^2}\right)^{1/5} y^{1/5}$$

When applying the parameters of the experimental study of Brodowicz and Kierkus (1966), one obtains $T(y) - T_0 = 1.28y^{-3/5}$ and $v(y) = 0.274y^{1/5}$. Fig. 16 displays the present numerical results on the symmetry line and the comparison with the solutions of Gebhart et al. (1970). A good agreement between the numerical and similarity solutions is observed for the temperature distribution. For the vertical velocity there is a small discrepancy which was also observed by Brodowicz and Kierkus (1966) from their experimental results. The present numerical simulation reproduces correctly these scaling laws.

4. Summary and concluding remarks

Laminar external convection induced by a line heat source was studied experimentally and numerically. The experiments were performed with a platinum wire of 50 μm in radius immersed in a large pool of water and heated with a constant heat flux and three different heat flux values were investigated. From simultaneous numerical and experimental investigations, the followings conclusions can be drawn:

1 Numerical and experimental comparisons allowed validating previously established scaling laws of $t \sim q^{-1/2}$, $\delta r \sim q^{-1/4}$ and $v \sim q^{1/4}$. Although these laws were derived from a scaling analysis of the early onset of convective motion, the present study shows that these laws are still valid at longer times.
2 Quantitative comparisons between the experiments and the corresponding numerical simulations were performed over the whole transient to address the reliability of the artificial conditions implemented on the boundary of the computational domain. Comparisons of velocity and temperature fields in the thermal plume have highlighted that from a computational standpoint three different stages must be distinguished:In the first stage the initial vortices are completely inside the computational domain. In this case, a good agreement is achieved between experiments and numerical simulations in the entire computational domain.The second stage starts when the initial vortices and the front of the thermal plume reach up to the edge of the computational domain and finishes when they have totally passed through the outer boundary. These values depend on the numerical parameters. During this second stage, a good agreement is achieved between experiments and numerical simulations away from the outflow boundary.In the ultimate stage, the initial vortices have left the computational domain and a quasi-steady laminar flow establishes around the wire. A good agreement between experimental and numerical results is achieved in the plume main stream as well as in the limited circle whose radius equals one-third of the computational domain radius.
3 Experiments showed that the centers of the initial vortices move along a linear path defined by $y = \mp 2.5 \times (x \pm 0.001)$. This trajectory is independent of the heat fluxes in the range investigated. A suitable numerical prediction of this trajectory is only achieved in the first stage, which is consistent with the aforementioned conclusion drawn for the second stage.
4 Lastly numerical simulations of steady laminar external natural convection induced by a thin wire 37.5 μm in radius heated in air were compared with an independent experimental study available in the literature. Despite a large wire superheat of about 210 K which breaks the Boussinesq assumption, a good agreement is obtained for temperature field except for a slight discrepancy in the symmetry plane. Furthermore, the numerical study recovers correctly the classical scaling laws of the far-field above the wire ($r >> R$): $v \sim y^{1/5}$ and $T - T_0 \sim y^{-3/5}$. As far as the steady flow structure is concerned, the main stream of the thermal plume is adequately described by numerical sim-

ulations. However experiments revealed that above the wire fluid is supplied horizontally to the plume. This specific feature is not properly reproduced by numerical simulations in which a spurious downward motion induced by the artificial boundary conditions is observed. Further work is required to improve this point.

More generally, this study shows that numerical simulations of transient external free convection can achieve quantitative agreement even if the numerical results cannot be expected to be correct everywhere in the whole computational domain. Only a limited region around the line heat source is likely to be properly described. Its extension depends on three parameters: the size of computational domain, the stage of transient free convection which depends both on the domain size and particularly on the artificial boundary conditions implemented at the outer boundary of the computational domain. It is clear that, with a fixed domain size, any hope to enlarge the region around the line source in which numerical results remain correct over transient stages 2 and 3 will require better artificial boundary conditions. In other words, more work on the mathematical modelling of artificial boundary conditions at the outer boundary and their numerical implementation is needed.

Acknowledgement

Computations have been performed at IDRIS (Institut du Développement et des Ressources en Informatique Scientifique) under Research Project 70326.

References

Bernardi, C., Maday, Y., 1992. Approximations spectrales de problèmes aux limites elliptiques. In: Collection Mathématiques & Applications. Springer-Verlag, Berlin.

Brodowicz, K., Kierkus, W., 1966. Experimental investigation of free-convection in air above horizontal wire with constant flux. Int. J. Heat Mass Trans. 9, 81–94.

Canuto, C., Hussaini, M., Quarteroni, A., Zang, T., 1988. Spectral Methods in Fluid Dynamics. Springer-Verlag, New York.

Corcione, M., 2005. Correlating equations for free convection heat transfer from horizontal isothermal cylinders set in a vertical array. Int. J. Heat Mass Trans. 48, 3660–3673.

Duluc, M.-C., Xin, S., Le Quéré, P., 2003. Transient natural convection and conjugate transients around a line heat source. Int. J. Heat Mass Trans. 46, 341–354.

Farouk, B., Güçeri, S., 1981. Natural convection from a horizontal cylinder—laminar regime. J. Heat Trans. 103, 522–527.

Gebhart, B., 1988. Buoyancy-induced Flows and Transport. Hemisphere.

Gebhart, B., Pera, L., Schorr, A.W., 1970. Steady laminar natural convection plumes above a horizontal line heat source. Int. J. Heat Mass Trans. 13, 161–171.

Guermond, J.-L., Quartapelle, L., 1998. On the approximation of the unsteady Navier– Stokes equations by finite element projection methods. Numer. Math. 80 (5), 207–238.

Kelkar, K., Choudhury, D., 2000. Numerical method for the prediction of incompressible flow and heat transfer in domains with specified pressure boundary conditions. Numer. Heat Trans. B 38, 15–36.

Kuehn, T., Goldstein, R., 1980. Numerical solutions to the Navier–Stokes equations for laminar natural convection about a horizontal isothermal circular cylinder. Int. J. Heat Mass Trans. 23, 971–979.

Linan, A., Kurdyomov, V., 1998. Laminar free convection induced by a line heat source and heat transfer from wires at small Grashof numbers. J. Fluid Mech. 362, 199–227.

Ostroumov, G., 1956. Unsteady heat convection near a horizontal cylinder. Soviet. Phys. Tech. Phys. 1 (12), 2627–2641.

Quénot, G., Pakleza, J., Kowalewski, T., 1998. Particle image velocimetry with optical flow. Exp. Fluids 25, 177–189.

Saitoh, T., Sajiki, T., Maruhara, K., 1993. Bench mark solutions to natural convection heat transfer problem around a horizontal cylinder. Int. J. Heat Mass Trans. 36, 1251–1259.

Smith, B., Bjorstad, P., Cropp, W., 1996. Domain Decomposition: Parallel Multilevel Methods for Elliptic Partial Differential Equations. Cambridge University Press, New York.

Stanislas, M., Okamota, K., Kähler, C., Westerweel, J., 2005. Main results of the second international PIV challenge. Exp. Fluids 39, 170–191.

Turner, J.S., 1979. Buoyancy Effects in Fluids. Cambridge University Press, London.

Wang, P., Kahawita, R., Nguyen, T., 1990. Numerical computation of the natural convection flow about a horizontal cylinder using splines. Numer. Heat Trans. A 17, 191–215.

Xin, S., Duluc, M.-C., Lusseyran, F., Le Quéré, P., 2004. Numerical simulations of natural convection around a line-source. Int. J. Numer. Method Heat Fluid Flow 14 (7), 828–848.